Z. Kristallogr. **221** (2006) 420–434 / **DOI** 10.1524/zkri.2006.221.5–7.420

High-pressure crystal chemistry of binary intermetallic compounds

Roman Demchyna, Stefano Leoni, Helge Rosner and Ulrich Schwarz*

MPI für Chemische Physik fester Stoffe, Nöthnitzer Str. 40, 01187 Dresden, Germany

In commemoration of the 100th anniversary of Fritz Laves' birthday

Received January 5, 2006; accepted February 10, 2006

High pressure / Binary intermetallic compounds / Crystal chemistry

Abstract. Effects of high pressure on intermetallic compounds are reviewed with regards to structural stability and phase transitions. Changes of bonding properties and electronic structure are examplified by means of the elemental metals caesium and titanium, the latter forming an internal intermetallic compound at high pressures. After a short systematic overview regarding pressure effects, structural transformations in selected classes of intermetallic compounds like Zintl phases and AlB_2-type arrangements precedes sections concerning high-pressure synthesis of Laves phases and intermetallic clathrates.

Introduction

Alloys and intermetallic compounds are among the oldest and most important man-made materials, being subject of constant interest for inorganic chemists, physicists and material scientists [1–9]. The basic difference between the two groups of phases is that alloys in general exhibit homogeneity ranges whereas intermetallic compounds are defined by a – at least in principle – definite composition.

One of the focal points in the chemistry of intermetallic compounds is the development of an understanding of systematic trends concerning phase stability, *e.g.*, by means of structure maps employing a large variety of different scales (see [10, 11] and references therein). In the context of investigating the realization of specific structural patterns and changes of chemical bonding in solids, high pressure is one of the fundamental state variables which can be varied in order to uncover factors governing stability fields of structure and bonding types as well as to separate electronic effects from packing aspects. Simultaneously, it is a useful parameter in quantum chemical investigations since the compression can be easily simulated in the calculations by a corresponding reduction of unit cell parameters.

* Correspondence author (e-mail: schwarz@cpfs.mpg.de)

In the following sections, electronic effects of high pressure application will be summarized before examples for the differentiation of atoms in high-pressure modifications of chemical elements are analysed in some detail for the metals caesium and titanium. A systematic categorization of pressure-induced changes precedes overviews of structural phase transitions in selected classes of samples, *i.e.*, Zintl phases with composition 1 : 1 and AlB_2-type arrangements. Sections on high-pressure syntheses of Laves phases and intermetallic clathrates follow.

Electronic effects of high pressure

Phase formation in strongly polar intermetallic compounds often causes a reduction of the density of states at the Fermi level which gives rise to the formation of a pseudo-gap or even a real band gap, *e.g.*, in CsAu [12–15]. If we neglect some special cases like strongly correlated systems, application of pressure normally increases orbital overlap and causes band broadening. The resulting reduction of the fundamental band gap in semiconductors and insulators is often labelled as metallization. A similar enhancement of band dispersion originates in series of homologous elements from the intensification of atomic interactions with atomic weight (Fig. 1a). Thus, compression frequently induces the formation of structural patterns typical for heavier group homologues, a finding which resulted in the formulation of the pressure homology rule (R. H. Wentorf, cited after [16]). However, some differences originate from the fact that, in contrast to increasing atomic weight, application of high pressure is not associated with an enhancement of relativistic effects and, within the stability fields of structural patterns, volume reduction by compression can be realized in a continuous way.

An empirical concept to translate the effects of chemical substitution into those of a compression is that of chemical pressure. Here, crystal chemical changes are attributed completely to the radius difference of the involved species. A shortcoming of this approach is that both chemical substitution and compression will alternate parallely size and electronic properties of the atoms. However, the pressure-induced changes of the electronic features will typically not correspond to those of the chemical substitution.

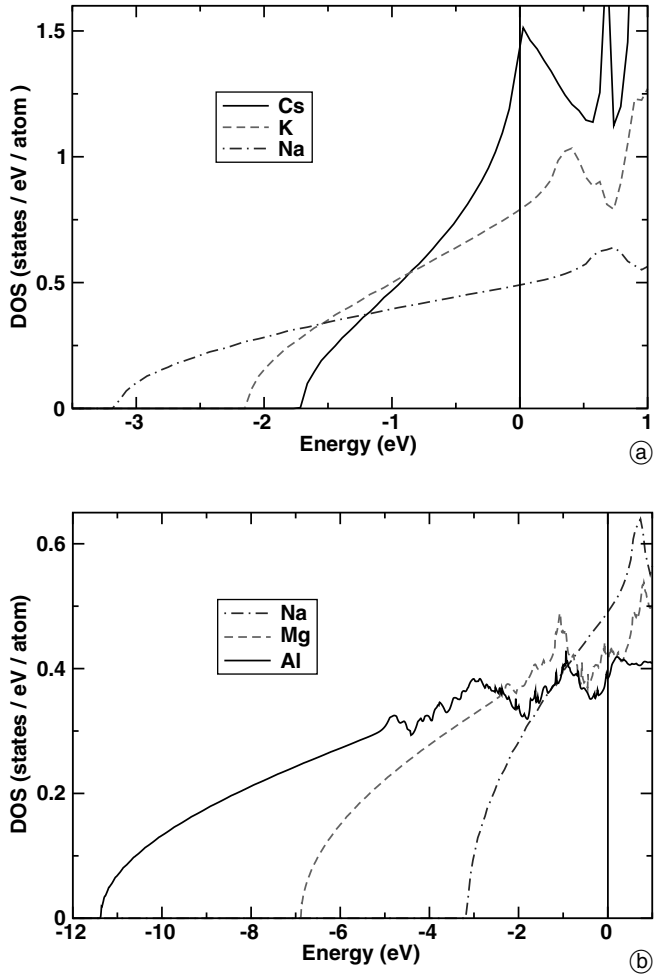

Fig. 1. Density of states (DOS) as revealed by density functional theory band structure calculations [21]. (**a**) Alkali metals sodium, potassium and caesium; (**b**) Third row main group metals sodium, magnesium and aluminium. For the heavy alkali metals, the DOS close to the Fermi level is modified by the presence of *d*-states, subtle deviations for magnesium and aluminium are attributed to the occupation of *p*-states.

Crystallographic differentation of atoms in elements

Some basic effects of high-pressure application will be recalled by employing main group elements as examples. Here, semiconductors like silicon (and binary Grimm-Sommerfeld compounds) exhibit pronounced pressure-induced structural phase transformations which are associated with dramatic electronic changes like insulator-metal transitions. However, structural patterns with metal-type conductivity can exhibit a significant amount of covalent bonding, *e.g.*, Si-VI [17, 18] adopting an atomic arrangement observed exclusively for high-pressure phases.

At ambient pressure, essential structural and electronic features of semimetals like arsenic (and isoelectronic binaries) result from symmetry-breaking which opens bandgaps at the zone bondary. Upon compression the Peierls-distorted semiconducting modifications (Jahn-Teller systems) undergo transformations into elemental metals (see *e.g.* [19]). These transitions are driven by band-broadening caused by the increasing overlap of *sp*-orbitals originating from the reduction of interatomic distances.

Most main group metals exhibit at ambient conditions a density of states (DOS) which is proportional to the square root of the energy, a finding which is in good agreement with a nearly free electron regime [20] as it is observed for, *e.g.*, elemental sodium at ambient pressure (see calculated DOS [21] in Fig. 1a). Proceeding within the second period from sodium via magnesium to aluminium reveals that all three elements are in good approximation nearly free electron metals (Fig. 1b). In both selected sets, intensification of next-neighbour interaction is reflected by increasing band dispersion. With increasing atomic weight of the metal, the density of states close to the Fermi energy is significantly modified by the presence of *d*-states [20]. Minor deviations for magnesium and aluminium can be attributed to the occupation of *p*-states.

However, a pressure-induced onset of covalent interactions in metals is possible and will be examplified by the phase changes of caesium. For visualization, we will employ the Electron Localization Function (ELF). The ELF was originally formulated in the Hartree-Fock approximation and is frequently used as a detector for covalent interactions [22]. In the density functional theory calculations we used the formulation of ELF within DFT [23] of the original expression [22]. A recently proposed more general functional called electron localizability indicator (ELI) [24] yields the average number of same-spin electron pair density in a small region with a fixed charge. In the Hartree-Fock approximation the Taylor expansion of the proposed localizability functional can be related to the ELF. Thus, ELF and ELI are considered as fingerprints of (covalent) bonding in real space.

Computations[1] of the ELF isosurface ($\eta = 0.35$) of the high-pressure phase Cs-IV reveal in accordance with earlier findings [28, 29] (Fig. 2a) localization domains of the outer-core basins of Cs atoms and bonding localization domains in the triangular prismatic interstices. The latter correspond to the Si sites in $ThSi_2$ [30]. On further lowering the interpolation value, the outer-core basins and the interstitial basins form a seperate basin set at $\eta = 0.37$. The interstitial basins get connected into an extended shape with the topology of the silicon substructure of $ThSi_2$ (Fig. 2a, ELF isosurface with $\eta = 0.24$).

Calculations of the ELF for Cs-V (Fig 2b) reveal maxima at the centers of octahedra in the 3D structure [31]. No

[1] In the scalar relativistic full-potential calculations with the FPLO method (full potential minimum basis local orbital scheme) [21], we used the exchange and correlation potential of Perdew and Wang [25]. For caesium, Cs(4*d*, 5*s*, 5*p*, 6*s*, 6*p*, 5*d*) states were chosen as basis sets. Lower lying states were treated as core states. The 5*d* states were taken into account to increase the completeness of the basis set. The inclusion of 4*d*, 5*s* and 5*p* states in the valence states was necessary to account for non-negligible core-core overlaps. The spatial extension of the basis orbitals, controlled by a confining potential [26] was optimized to minimize the total energy. A *k*-mesh of 244 points (Cs-IV) and 456 points (Cs-V) in the irreducible part of the Brillouin zone was used. Convergency with respect to *k*-points and basis sets were carefully checked. For the titanium modifications, Ti(3*s*, 3*p*, 4*s*, 4*p*, 3*d*) states were selected as basis sets. A *k*-mesh of 144 points (α-Ti) and 192 points (ω-Ti) in the irreducible part of the Brillouin zone was used. For the calculation of the ELF the FPLO ELF-module was used [27].

other maxima apart from the outer-core basins are appearing. ELF evidences the formation of clusters, a new feature that was still absent in Cs-IV and which is a signature of the increased participation of *d*-orbitals in the bonding [17].

The increasing directional bonding character of the compressed alkali metals shows in low-symmetry atomic arrangements with unusual coordination numbers. It is attributed to pressure-induced increases of the occupation of *p*-states for the light homologues (lithium [32] and sodium [33]) and a corresponding s–d transition for the heavy homologues (rubidium and caesium [34]). Similar s–d transitions upon compression have been formulated for the alkaline earth metals Ca [35], Sr and Ba [36] as well as for early transition metals like lanthanum [37].

Pressure-induced changes of the electron configuration and symmetry breaking phase transitions of elemental metals can result in a crystallographic differentation of chemically and physically identical atoms [see, *e.g.*, 38–44]. In other words, there is only a gradual difference between these high-pressure modifications and binary intermetallic compounds.

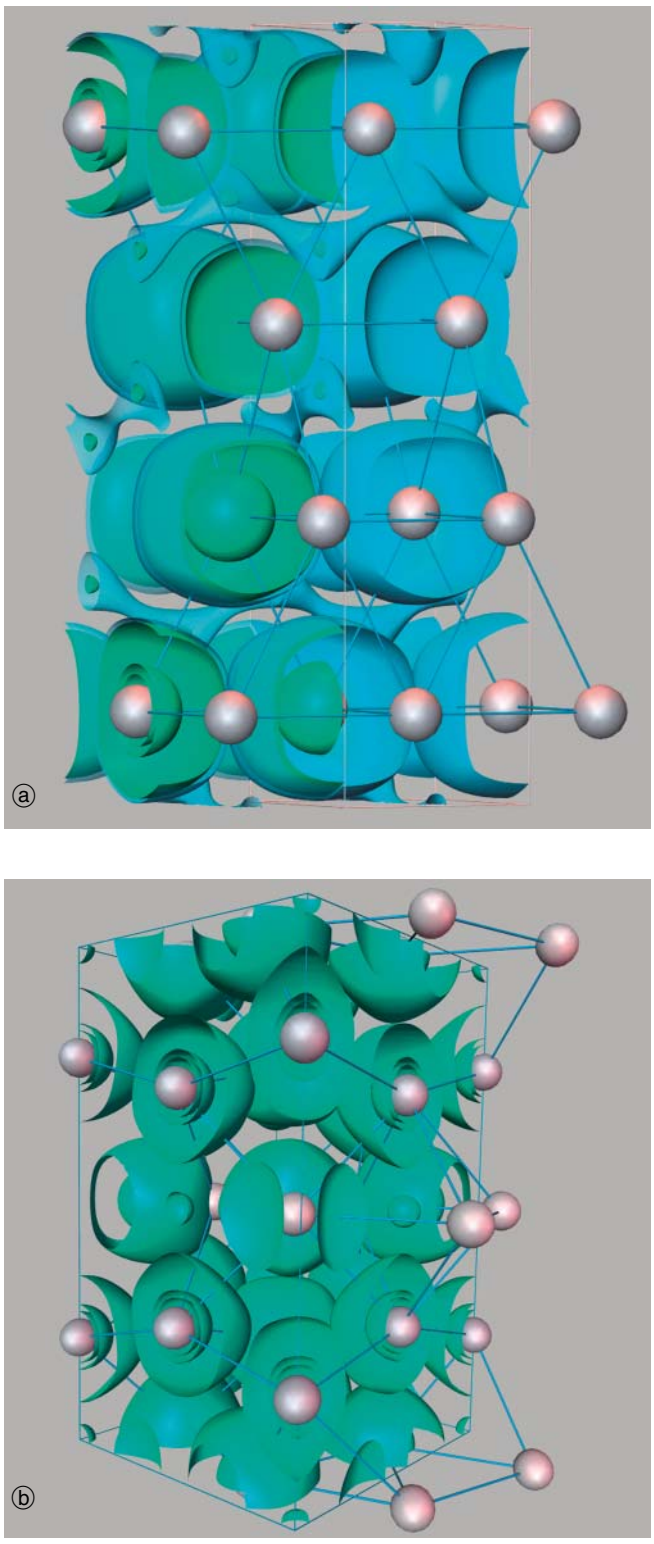

Fig. 2. Electron localization function of high-pressure modifications of caesium. (**a**) Cs-IV isosurface at $\eta = 0.35$ (green) and $\eta = 0.24$ (blue), (**b**) Cs-V, isosurface at $\eta = 0.34$.

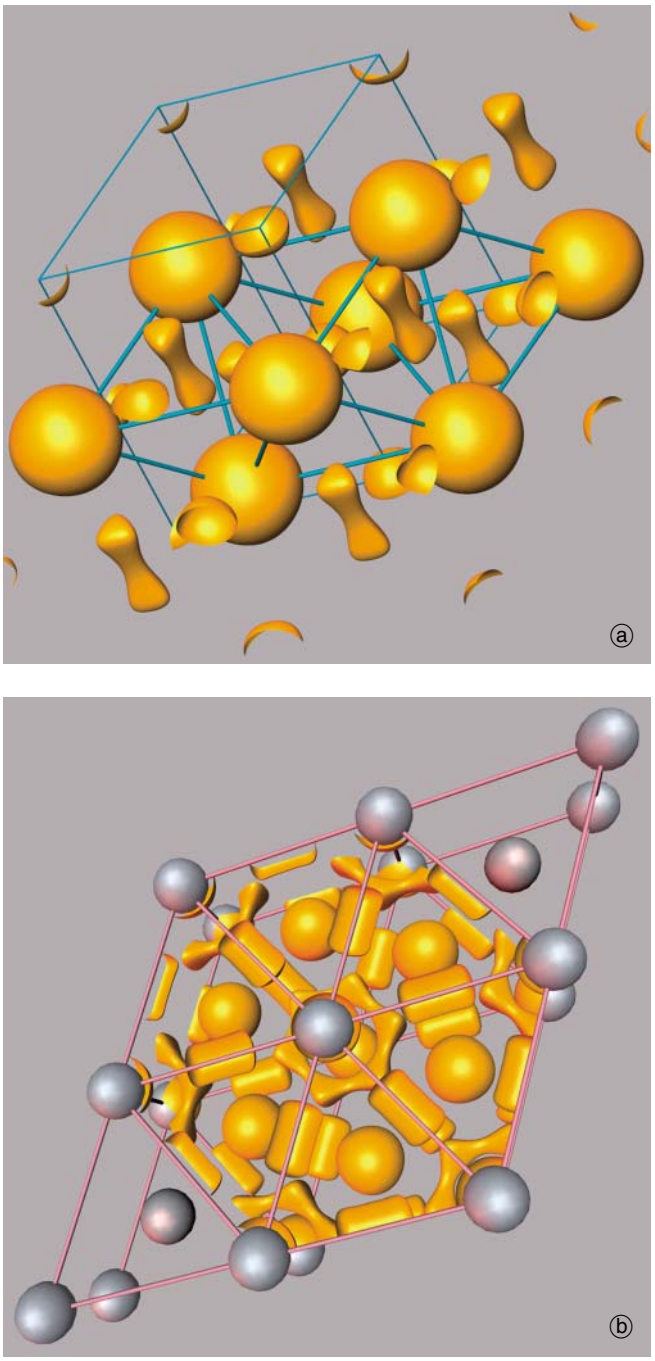

Fig. 3. Electron localization function of titanium modifications. (**a**) α-Ti, isosurface at $\eta = 0.65$, (**b**) ω-Ti, isosurface at $\eta = 0.65$.

This phenomenon will be further illustrated by the so-called ω-phases and the high-pressure polymorphism of titanium [45–49]. The ELF of α-Ti shows outer-core basins above the value $\eta = 0.76$ (Fig. 3a). Interstitial basins appear for lower values. At $\eta = 0.76$ attractors are visible in the octadedral voids, additional extrema show up in the tetrahedral voids at $\eta = 0.71$ and these basins interconnect at $\eta = 0.69$. All bonding basins fuse into a common set at $\eta = 0.46$. The attractors in the valence region are four- or six-synaptic revealing the multi-center character of bonding [50].

For the high-pressure modification ω-Ti [45–49], the ELF shows at $\eta = 0.79$ cylindrical localization domains in the a, b hexagonal plane which are located on shortest contacts between Ti_1 atoms thus indicating two-center bonding (Fig. 3b). Additionally, six basins (attractor at $\eta = 0.75$) interconnect to form a torus topology ($\eta = 0.69$) oriented around the Ti_1-Ti_1 connections along [001]. The Ti_2 positions are separated from the Ti_1 partial structure by minima in the ELF. They occupy triangular prismatic interstices in a network of covalently bonded Ti_1 atoms. The axial bond attractors with toroid-like basin sets are reminiscent of the ring attractors in the molecules ScGa and Sc_2 [51]. Both attractors reveal directed (covalent) interactions within the Ti_1 substructure which are confirmed by the density of state computations.

In the total and projected DOS (see Fig. 4) of α-Ti the lower part of the region between -6 eV and the Fermi level is shaped by 4s states, while 4p and 3d states are more pronounced in the upper part. The hybridization of 4s and 4p orbitals with 3d orbitals is only partial, and this region is dominated by d states. Higher pressure only slightly increases the dispersion of this region of the DOS. Much more, it affects the mixing-in of 4s and 4p states into 3d states, and to a different extent for the two Ti crystallographic sites. While for Ti_2 (interstitial) the contribution of 4s and 4p to the region just below the Fermi level is similar to the situation in α-Ti, for Ti_1 the mixing-in of 4s and 4p states has strongly increased. The signature of the hybridization occurring at Ti_1 is given in the ELF by the pronounced structuring of its valence region. The changes of the hybridization together with the ELF justify the interpretation of ω-Ti as an internal intermetallic compound. A population analysis [52, 53] assigns a charge of $+0.5$ to Ti_2 and the high-pressure modification of titanium may be more precisely formulated as $((Ti_2)_2)^{+}Ti_1^{-}$. This charge distribution is in accordance with the observation that upon compression mixtures of electropositive potassium and electronegative silver in the ratio 2 : 1 react to form a binary compound K_2Ag adopting an ω-phase type atomic arrangement [54].

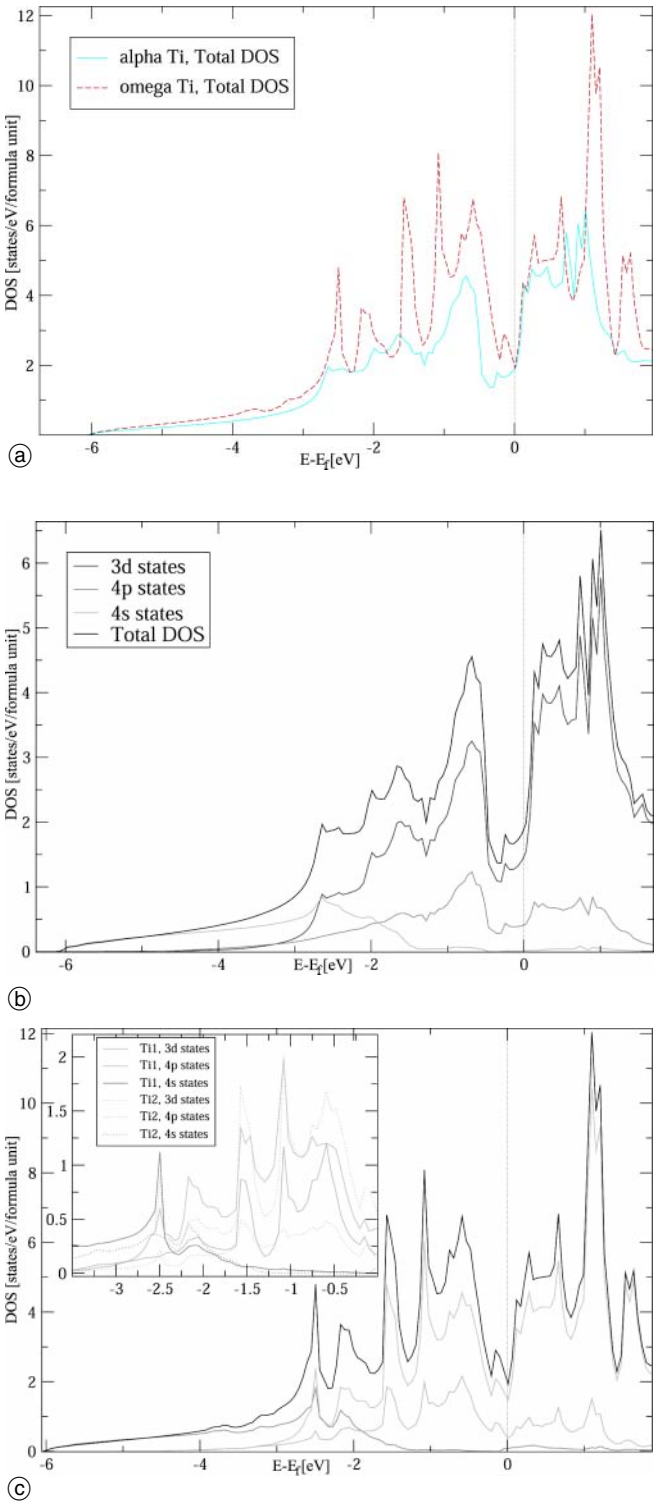

Fig. 4. Density of states of the low- (α) and high-pressure (ω) modifications of titanium. (**a**) Total DOS of α- and ω-Ti; (**b**) partial DOS of α-Ti; (**c**) partial DOS of ω-Ti.

Systematics of high-pressure effects

Summing up the findings of the last two sections from the viewpoint of crystal chemistry, metallic high-pressure modifications of elements can be categorized into four groups: (i) unique atomic arrangements adopted at high-pressure conditions, (ii) realization of crystal structures of heavier group homologues, (iii) formation of patterns which are observed for intermetallic compounds, or (iv) partial structures thereof.

With respect to experimental conditions, high-pressure experiments are either in-situ investigations or high-pressure syntheses of (meta-)stable phases. The second group of experiments is typically performed with element mixtures which segregate into two or more phases when solidified at ambient pressure.

Taking into account the crystal chemical and electronic effects of high pressure, the following groups of experiments on intermetallic compounds result:

a) Continuous alterations of the crystal structure upon compression (*e.g.* [55–62]).
b) Pressure-induced electronic changes, *e.g.*, oxidation state changes of the potentially valence instable rare-earth metals ytterbium, europium and cerium. Pressure-driven *s*–*d* (or *s*–*p*) transitions like in the alkali- and alkaline-earth metals or the early transition metals (see above) are expected for weakly polar intermetallic compounds of these elements. Finally, suppression of magnetic interactions due to band broadening is anticipated for magnetically ordered phases.
c) Pressure-induced structural phase transitions which are normally associated with a discontinuous increase of density. These transitions are frequently (but not necessarily) associated with an increase of coordination number (Pressure-coordination rule, M. Buerger, cited after [16]).
d) Stabilization of compounds adopting compositions which are thermodynamically unstable at ambient pressure.
e) Phase formation by compression of mixtures which exhibit an immiscibility gap at ambient pressure, *e.g.*, the binary systems Yb–Mn, Yb–Fe, Yb–Ni and Yb–Co.
f) High-pressure high-temperature syntheses and crystal growth experiments of compounds constituted from elements differing largely in their vapour pressure at the synthesis temperature.

The microscopic driving force for phase formation at high-pressures is not explicitly investigated in the majority of studies on intermetallic compounds. However, the total energy changes associated with the realization of different atomic arrangements amount to typically less than one percent of the cohesive energy. The available data invite to order the condensed overviews in the tables according to composition and crystal chemistry of the phases. We like to note here that pressure-induced subtle distortions of crystal structures which are evidenced by anomalies of physical properties but not characterized by diffraction methods will not be considered in the tables (*e.g.* [63]). For clarity, high-pressure syntheses of phases which also form at ambient pressure will be omitted (*e.g.* [64–66]). In the following sections, references to the original work are given in the corresponding tables.

Zintl phases with composition 1 : 1

Several of the investigated intermetallic compounds are strongly polar Zintl-phases comprising anionic partial structures with covalent bonding between main group metal atoms (Table 1). Among these, the NaTl structure can be described as a decoration variety of a cubic primitive lattice which represents an alternative to the CsCl-type pattern. In the cubic structure of NaTl each type of atom is surrounded tetrahedrally by four atoms of the same type thus forming a diamond-like net. An isostructural network of the second atom type is shifted by ($^1/_2$, $^1/_2$, $^1/_2$) so that the first coordination sphere of all atoms is completed by a second tetrahedron. The resulting coordination cube shows an alternating occupation of the vertices according to $A_{4/8}B_{4/8}$. In addition to these eight shortest distances equal to $a\sqrt{^3/_2}$ (a = lattice parameter of the cubic unit cell) six additional atoms are located at the slightly longer distance a (+15%). In the CsCl-type high-pressure modification, each atom is surrounded by eight unlike atoms at $a\sqrt{^3/_2}$ plus plus six atoms of the same type at the slightly longer distance a. The networks of both atom types form cubic primitive substructures in the high-pressure phase. The transformation proceeds via a reconstruction (LiIn) or two consecutive order-disorder transitions (NaTl – *cp* – CsCl). Since low- and high-pressure modification can be described as decoration variants of a cubic primitive lattice the coordination number is conserved throughout the structural change. The driving force of the phase transition is that with increasing pressure Madelung contributions favouring a CsCl arrangement become larger than the band structure stabilization due to homonuclear bonding within the anionic partial structure of the NaTl-type modifications [67].

A number of binary alkali metal silicides and germanides with 1 : 1 composition adopt the KGe structure type (Fig. 5) comprising P_4-analoguous tetrahedral units T_4^{4-} (T = Si, Ge) with short Ge–Ge or Si–Si distances at low pressure. The atomic pattern of the aristotype can be described as a stacking of very distorted centered octahedra $Ge[K_6]$ where the edges of the octahedra permeated with Ge–Ge bonds are larger than the closed edges. The lengths of the edges differ by as much as approximately 60%. The octahedra are connected by sharing vertices so that each K atom belongs to six different octahedra. On the other hand, the aggregate of K atoms in the first coordination sphere of $[Ge_4]$ tetrahedra forms a 16 vertices cluster. The high-pressure modification of KGe is iso-

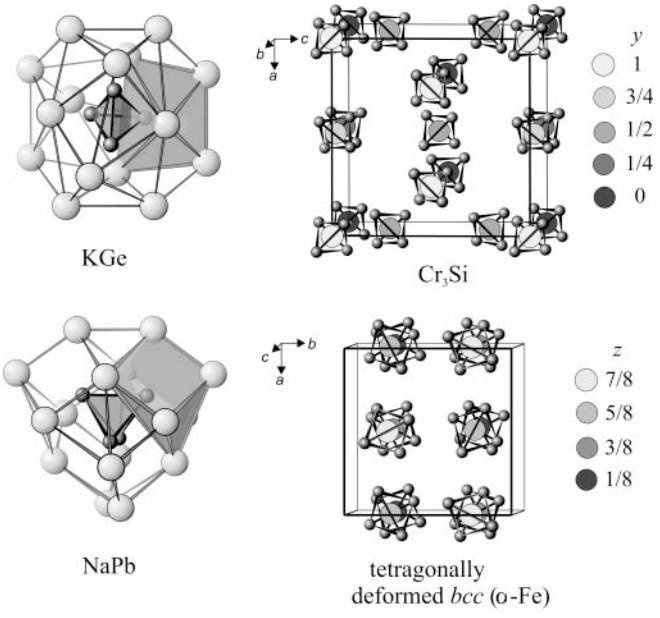

Fig. 5. Crystal structure of the low-pressure modification of KGe (own structure type) and the high-pressure modification (NaPb-type crystal structure): The different arrangements of $Ge_4[K_{16}]$ clusters and the location of centers of $[Ge_4]$ tetrahedra are shown.

Table 1. Pressure-induced phase transitions and high-pressure syntheses of intermetallic compounds with 1 : 1 composition.

Compound of type AB	Structure type low-pressure phase	Transition or synthesis conditions	Structure type high-pressure phase	Lit.
LiIn	NaTl	11 GPa	CsCl	70
KTl		2 GPa	NaTl	71
LiSi		4 GPa, 873 K	MgGa	72
KSi	KGe	4 GPa, 973 K	NaPb	73
RbSi	KGe	4 GPa, 973 K	NaPb	73
CsSi	KGe	4 GPa, 973 K	NaPb	73
FeSi	FeSi	24 GPa, 1950 K	CsCl	74
LiGe	MgGa	4 GPa, 773 K	HP-LiGe I	75
LiGe	MgGa	4 GPa, 1173 K	HP-LiGe II	76
NaGe	NaGe	4.GPa, 973 K	NaPb	77
KGe	KGe	4 GPa, 973 K	NaPb	73
RbGe	KGe	4 GPa, 973 K	NaPb	73
CsGe	KGe	4 GPa, 973 K	NaPb	73
MnGe		4–5 GPa, 1273–873 K	FeSi	78
CoGe	CoGe	7.7 GPa, 1623–773 K	FeSi	79
RhGe	MnP	7.7 GPa, 1623–773 K	FeSi	79
BaSn	TlI	4 GPa, 973 K	CsCl	80
LaP	NaCl	24 GPa	MnHg	81
CeP	NaCl	25 GPa	CsCl	81, 82
PrP	NaCl	26 GPa	MnHg	81
NdP	NaCl	30 GPa	MnHg	81
SmP	NaCl	35 GPa		81
GdP	NaCl	40 GPa		81
TbP	NaCl	38 GPa		81
TmP	NaCl	53 GPa		81
YbP	NaCl	51 GPa		81
YbAs	NaCl	52 GPa		83
LaSb	NaCl	11 GPa	MnHg	84
CeSb	NaCl	10 GPa	MnHg	84
PrSb	NaCl	13 GPa	MnHg	85
NdSb	NaCl	15 GPa	MnHg	85
SmSb	NaCl	19 GPa	MnHg	85
GdSb	NaCl	22 GPa	MnHg	85
TbSb	NaCl	21 GPa	MnHg	85
YbSb	NaCl	13 GPa	CsCl	82
CeBi	NaCl	13 GPa	CsCl	86
CeBi	NaCl	13 GPa	MnHg	86
PuBi	NaCl	10 GPa	*bct*	87
PuBi	*bct*	42 GPa	CsCl	87
TmTe	NaCl	8 GPa	TmTe	88, 89
TmTe	TmTe	15 GPa	NiAs	90
TmTe	TmTe	35 GPa		89
GdCu	CsCl	12.8 GPa	CdAu	91
LaAg	CsCl	5 GPa	CdAu	91
NdAg	CsCl	3.4 GPa	CdAu	91
AgZn	*trig*-ζ	3.1 GPa	CsCl	92
NdZn	CsCl	4.2 GPa	CdAu	91
CeZn	CsCl	2 GPa	CdAu	91
LiCd	NaTl	11 GPa	CsCl	70

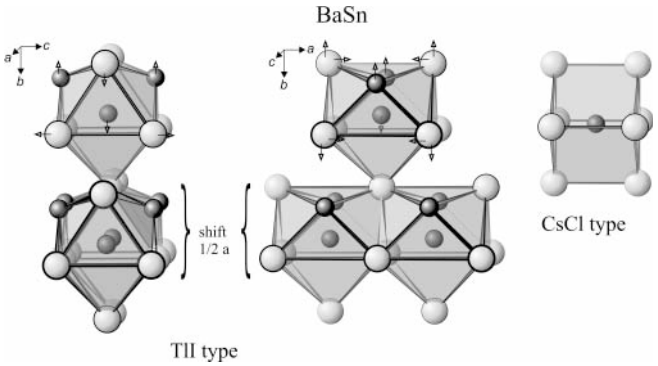

Fig. 6. Crystal structure of the low pressure modification of BaSn (TlI-type crystal structure) and the high-pressure modification (CsCl type): The phase transition can be described as a shift of columns of trigonal prisms relative to neighboring columns and synchronous displacements of atoms (indicated by arrows).

structural to NaPb and similar to the KGe type due to the existence of potassium atoms arranged around [Ge_4] tetrahedra. The two modifications differ by the spatial organisation of the potassium atoms and by the cluster condensation. The surrounding of Ge atoms in high-pressure KGe is a polyhedron with CN7 which is pronouncedly less regular than the octahedra in the crystal structure of low-pressure KGe. The centers of the [T_4] tetrahedra form a distorted structure of an α-Fe-type in case of high-pressure KGe (NaPb type) and a β-W-type (Cr_3Si-type) arrangement in case of the ambient pressure modification.

A more substantial structural reorganization is observed for the corresponding lithium compound LiGe. The low-pressure modification forms a 3D network of three-bonded germanium. Upon compression, two different high-pressure phases of LiGe are formed. A hexagonal one comprises six-membered rings of (3b)Ge^- which are condensed to channels along [001]. The second high-pressure phase consists of corrugated layers of two- and four-bonded germanium. According to the (8-N) rule, the formation of this phase is associated with a pressure induced disproportionation of (3*b*)Ge^- into (4*b*)Ge^0 and (2*b*)Ge^{2-}. However, with regard to the charge balance the second modification is electron deficient since it contains twice as many (2*b*)Ge^{2-} as (4*b*)Ge^0.

The crystal structure of the low-pressure modification of BaSn is isostructural to TlI (Fig. 6). The atomic pattern can be regarded as an arrangement of trigonal prisms Sn[Ba]$_6$ and empty tetragonal pyramids [Ba]$_5$ resulting in a coordination number of 7 for both atom types. At high pressure there is a phase transition into the CsCl-type with CN 8 for both atom types. Formally, the transition can be described as a shifting of columns of trigonal prisms along their three-fold axis by a translation $^1/_2a$ relative to the neighbouring columns associated with synchronous shifts of the atomic positions until a CsCl-type arrangement is realized.

High-pressure phases of AlB_2-type compounds

Another frequently observed atomic pattern of intermetallic phases are AlB_2-type structures and distorted varieties

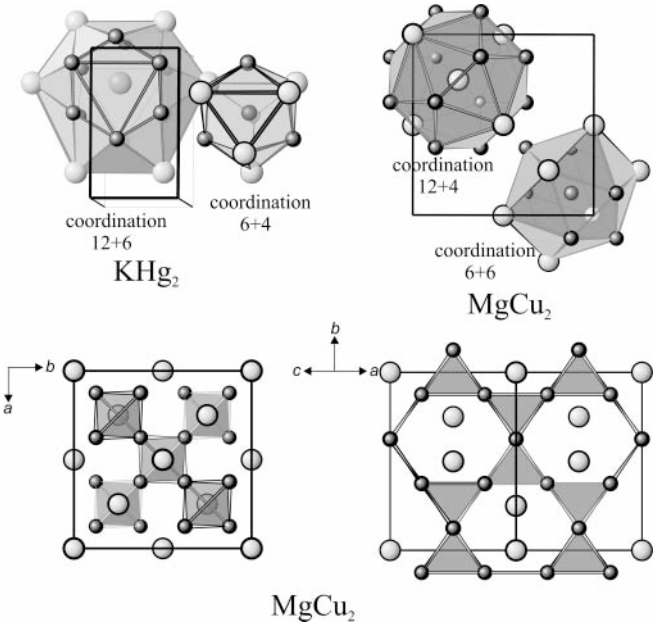

Fig. 7. Crystal structure of the low-pressure modification of $SrAl_2$ (KHg_2-type crystal structure, see also Fig. 8) and the high-pressure modification ($MgCu_2$-type Laves phase): Coordination polyhedra of the structure types (top) and two projections of the tetrahedral framework in the Laves phase (bottom) are shown.

thereof (Table 2). In the aristotype, B atoms form regular hexagonal planar (graphite-like) nets with three bonded atoms. In the very frequent distortion variety of the KHg_2 type, the graphitic nets are corrugated in a special way resulting in a 3D polyanionic mercury network of four-bonded atoms (Fig. 8). At high pressures, the orthorhombic crystal structure of KHg_2 (space group *Imma*, $Z = 4$) tranforms into the more symmetrical hexagonal crystal structure of the AlB_2 type (see Table 2) with a *c*/*a* ratio of approximately 0.6. The same type of transition is observed in the rare-earth metal digallide $TmGa_2$. It was shown by bandstructure calculations and bonding analysis that the

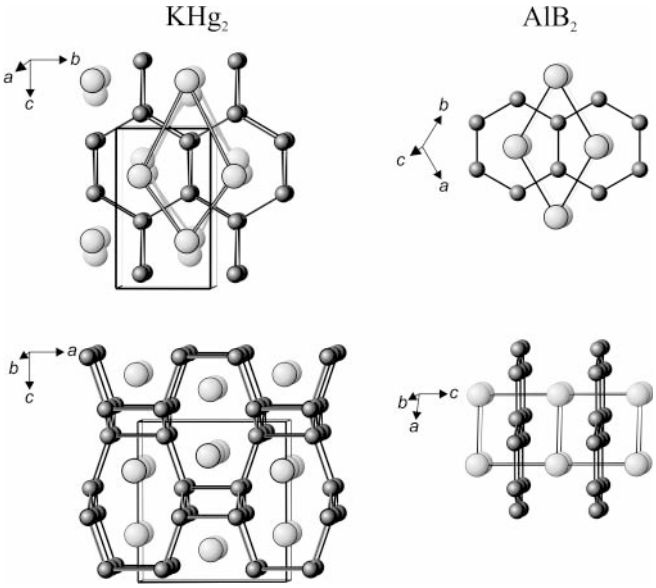

Fig. 8. Crystal structure of the low-pressure modification of KHg_2 (own structure type; also labeled as $CeCu_2$ type) and the high-pressure modification (AlB_2-type crystal structure): The pressure-induced transition transforms corrugated Hg layers into planar slabs.

Table 2. High-pressure phase transitions and syntheses of intermetallic compounds with 1 : 2 composition.

Compound of type AB_2	Structure type low-pressure phase	Transition or synthesis conditions	Structure type high-pressure phase	Lit.
$ScGa_2$	KHg_2	2.5–7.7 GPa, 473–1273 K	$ZrGa_2$	93
$CeGa_2$	AlB_2	16 GPa	*Hexagonal*	94
$HoGa_2$	AlB_2	4 GPa	$AlB_2/CaIn_2$	95
$TmGa_2$	KHg_2	22 GPa	AlB_2	96
$YbGa_2$	$CaIn_2$	22 GPa	AlB_2	97
$OsGa_2$		7.7 GPa, 570 K	$TiSi_2$	98
$CdGa_2$	AlB_2	7.7 GPa	AlB_2	99
$AuIn_2$	CaF_2	8 GPa	*Distorted* Co_2Si	100
Mg_2Si	CaF_2	2 GPa, 1773 K	*Hexagonal*	101, 102
$CaSi_2$	$CaSi_2$	4 GPa, 1273 K	α-$ThSi_2$	103
$CaSi_2$	$CaSi_2$	9 GPa	*Trigonal*	104
$CaSi_2$	*Trigonal*	16 GPa	AlB_2	104
$SrSi_2$	$SrSi_2$	4 GPa, 1273 K	α-$ThSi_2$	103
$BaSi_2$	$BaSi_2$	4 GPa, 1273 K	α-$EuGe_2$	105
$BaSi_2$		3.5 GPa, 873 K	$SrSi_2$	105
Mg_2Ge	CaF_2	2 GPa, 1773 K	*Hexagonal*	101, 102
$SrGe_2$	$BaSi_2$	1.4 GPa, 1073 K	$EuGe_2$	106
$BaGe_2$	$BaSi_2$	4 GPa, 1273 K	α-$ThSi_2$	107
$MoGe_2$	Co_2Si	0.8–7.8 GPa, 670–1220 K	$MoSi_2$	108, 109
WGe_2		$\leq$3 GPa, 873 K	Co_2Si	110
WGe_2		2.5–7.7 GPa, 1773–2773 K	$MoSi_2$	110
$NiGe_2$		5.5 GPa, 973 K	$CoGe_2$	111
Mg_2Sn	CaF_2	5.2 GPa, 1670 K	Mg_9Sn_5	112
$PtSn_2$	CaF_2	2.5–7.5 GPa, 800–1600 K	*Tetragonal*	113
$PtPb_2$		7.7 GPa, 1570–1770 K	$CuAl_2$	114
YSb_2		5 GPa, 873–1973 K	$HoSb_2$	115
$GdSb_2$		2–4 GPa, 1273–1773 K	$LaSb_2$	115
$GdSb_2$		4.5 GPa, 773–1573 K	$HoSb_2$	115
$TbSb_2$		3–4 GPa, 1273–2073 K	$LaSb_2$	115
$TbSb_2$		4 GPa, 773–1773 K	$HoSb_2$	115
$DySb_2$		3 GPa, 1173–1973 K	$HoSb_2$	115
$HoSb_2$		4 GPa, 773–1973 K	$HoSb_2$	115
$ErSb_2$		4 GPa, 773–1773 K	$HoSb_2$	115
$TmSb_2$		5 GPa, 773–1973 K	$HoSb_2$	115
$GrSb_2$	FeS_2	5.5 GPa	$CuAl_2$	116
$NiSb_2$	FeS_2	6 GPa, 923 K	$NiAs_2$	117
Na_2Te	CaF_2	2.3 GPa	$PbCl_2$	118
Na_2Te	$PbCl_2$	5.3 GPa	Ni_2In	118
$LaCu_2$	AlB_2	1.6 GPa	KHg_2	119
K_2Ag		4 GPa	AlB_2	54
KHg_2	KHg_2	2.5 GPa	AlB_2	120
$MgEr_2$		1.5 GPa, 2023 K	$MoSi_2$	121
$MgTb_2$		1.5 GPa, 1953 K	$MoSi_2$	121

structural change is associated with a breaking of gallium–gallium bonds. Thus, gallium is transformed from four-bonded in the 3D network of the low-pressure modification to three-bonded in the layers of the high-pressure modification.

A closely related transition mechanism from a distorted AlB_2 variety into the undistorted AlB_2 aristotype is observed for $YbGa_2$ at high pressures. Here, the low-pressure $CaIn_2$-type structure with four-bonded gallium atoms transforms into an AlB_2-type atomic arrangement with three-bonded gallium at high pressure. Compression and structural transition are paralled by a change of the rare-earth metals oxidation state from Yb^{2+} at low pressure towards Yb^{3+} in the high-pressure form. Consequently, the structural change in the anionic network can be described as an internal redox reaction from $(4b)Ga^{-}$ into $(3b)Ga^{1.5-}$.

A slightly different transition is observed for the AlB_2 type rare-earth metal digallides $GdGa_2$ and $CeGa_2$. Here, a

structural phase transition is associated with a discontinuous decrease of the *c*/*a*-ratio and a conservation of the topology of the gallium nets, *i.e.*, three-bonded gallium in both the low- and the high-pressure modification. At ambient pressure, the covalent character of the intralayer Ga-bonding causes short interatomic distances and, thus, a small lattice parameter *a*. This shortening of the *a*-axis has to be compensated for by an elongation of the *c*-axis since the distances between the network atoms and the rare-earth metal atoms between the layers are determined by the sum of the atomic radii. Thus, large *c*/*a*-ratios (typically around one) result at low pressures. The phase transition is associated with a strong discontinuous decrease of the interlayer non-bonding distances along [001] (8% for $GdGa_2$) while the intralayer gallium−gallium bond distances along [100] increase (2.5% for $GdGa_2$). As a result, the high-pressure phases which are often labelled as UHg_2-type atomic arrangements exhibit *c*/*a* ratios which are reduced by about 10%. Despite the pronounced shortening of the non-bonding gallium-gallium distances, the pressure-induced reduction is not sufficient to allow for a significant strengthening of the interlayer interactions. In the context of these pressure-induced phase-transition of AlB_2 varieties, the structural change of $LaCu_2$ (AlB_2 type at 1.6 GPa, KHg_2 type at 3.9 GPa) is a suitable candidate for investigations of bonding properties in strongly polar transition metal compounds.

Table 3. High-pressure modifications with Laves phase crystal structures.

Compound of type AB_2	Structure type low-pressure phase	Transition or synthesis conditions	Structure type high-pressure phase	Lit.
$HoMg_2$		1.4 GPa, 2023 K	$MgZn_2$	122
$TmMg_2$		1.4 GPa, 1973 K	$MgZn_2$	122
$YbMg_2$		1.4 GPa, 1473 K	$MgZn_2$	122
$SrAl_2$	KHg_2	6 GPa, 1323 K	$MgCu_2$	123
$BaAl_2$		3 GPa, 1273 K	$MgCu_2$	124
$ThAl_2$	AlB_2	0.3 GPa	$MgCu_2$	125
UAl_2	$MgCu_2$	11 GPa	$MgNi_2$	126
$EuPd_{0.72}In_{1.28}$		10.5 GPa, 1500 K	$MgZn_2$	127
$EuPt_{0.56}In_{1.44}$		10.5 GPa, 1400 K	$MgZn_2$	127
YMn_2	$MgCu_2$	7 GPa, 2273 K	$MgZn_2$	128
$GdMn_2$	$MgCu_2$	7 GPa, 2273 K	$MgZn_2$	128, 129
$TbMn_2$	$MgCu_2$	7 GPa, 2273 K	$MgZn_2$	128, 129
$DyMn_2$	$MgCu_2$	7 GPa, 2273 K	$MgZn_2$	128, 129
$YbMn_2$		7.7 GPa, 1623 K	$MgZn_2$	130, 131
UMn_2	$MgCu_2$	3 GPa	*Orthorhombic*	132
$PrFe_2$		2.8–5.0 GPa, 973 K	$MgCu_2$	133, 134
$Pr_{1-x}R_xFe_2$, R = Ce, Nd		2.8–5.0 GPa, 973 K	$MgCu_2$	135
$NdFe_2$		2.8 GPa, 1623 K	$MgCu_2$	131
$SmFe_2$	$MgCu_2$	7.7 GPa, heating	$MgZn_2$	133
$GdFe_2$	$MgCu_2$	7.7 GPa, heating	$MgZn_2$	133
$TbFe_2$	$MgCu_2$	7.7 GPa, heating	$MgZn_2$	133
$HoFe_2$	$MgCu_2$	7.7 GPa, heating	$MgZn_2$	133
$YbFe_2$		7.7, 0.6 GPa, 1623 K	$MgCu_2$	131, 136
$LuFe_2$	$MgCu_2$	7.7 GPa	$MgZn_2$	133
YFeCu		7.7 GPa, heating	$MgCu_2$	137
GdFeCu		7.7 GPa, heating	$MgCu_2$	137
$Yb(Fe_{1-x},Cu_x)$		7.7 GPa, heating	$MgCu_2$	137
$NdRu_2$	$MgCu_2$	7.8 GPa, 1503 K	$MgZn_2$	138
$SmRu_2$	$MgCu_2$	0.6 GPa, 1503 K	$MgZn_2$	138
$LaOs_2$	$MgCu_2$	6–14 GPa, 1050 K	$MgZn_2$	139
$CaCo_2$		8 GPa, heating.	$MgCu_2$	140
$Ca(Fe_{1-x}Ni_x)_2$		8 GPa, heating	$MgCu_2$	141
$LaCo_2$		1–6.5 GPa, 1323–1623 K	$MgCu_2$	142
KAg_2		7–40 GPa, 2300 K	$MgZn_2$	143
KAu_2		4 GPa, 1075 K	$MgZn_2$	144
$NaPt_2$		4 GPa, 1650–1050 K	$MgCu_2$	145
$ScZn_2$		4 GPa, 2173 K	$MgZn_2$	146

High-pressure Laves phases

A pressure-induced transition from a KHg_2-type valence compound into a metallic Laves phase with a cubic $MgCu_2$-type arrangement is observed for $SrAl_2$ (Table 3 and Fig. 7). In the low-pressure arrangement the majority species (4*b*)Al forms a 3D anionic framework by a specific distortion of hexagonal nets. The four-bonded anion Al^- is in accordance with an electron precise Zintl phase fulfilling the (8-N) rule.

In the $MgCu_2$-type crystal structure, the majority atoms form a framework by vertex-sharing of empty tetrahedra $[Al_4]$. As a consequence, the transformation is associated with an increase of the average number of homonuclear aluminium contacts since the four-bonded species is transformed into four- and six-bonded ones which are located in the bases and the tips of the tetrehedra, respectively. The structural change is associated with an increase of coordination number from 10 to 12 for aluminium. This reconstructive transition of $SrAl_2$ follows the same systematic trend from a polyanionic Zintl-phase at low pressures into an intermetallic compound at high pressures as the transformations of LiIn and LiCd. Synthesis of the analoguous barium compound $BaAl_2$ also requires high-temperature high-pressure conditions while at atmospheric pressure the aluminium richest phase is Ba_7Al_{13}.

The large number of Laves phases forming at high-pressures is attributed to the formation of topological close-packings of two atom types with similar electronegativity and a size ratio of $1:\sqrt{1.5}$ (r_A/r_B approximately 1 : 1.225) in the idealized molar ratio of 1 : 2 (for a recent review of stabilizing factors, see [68]). The importance of radius ratios for the packing of unlike atoms is strikingly underlined by the experimental observation of the solid noble gas compound $NeHe_2$ with a $MgZn_2$-type Friauf Laves phase crystal structure at high pressures [69].

However, the importance of directional bonding in some hexagonal Laves phases is clearly indicated by axial ratios which strongly deviate from the values found for an ideal close packing of spherical atoms. One of the extreme examples is KAu_2 which does not only exhibit a significant deviation of the radius ratio $r(K)/r(Au) = 1.648$ from the ideal value (1.225) but also a remarkable *c*/*a* ratio of 1.741 (ideal 1.633) and a difference of electronegativity corresponding to 1.5. Consequently, the rules concerning radius ratios are often soft with respect to a large number of inconsistencies or exceptions. One of the reasons for this is that charge transfer and size alterations are not taken into consideration. However, electron transfer may change the size and the shape of the constituting species significantly – especially in case of larger electronegativity differences.

Table 4. High pressure syntheses of binary or pseudo-binary clathrates and clathrate-like compounds with 3D anionic frameworks.

Composition	Synthesis conditions	Structure type	Lit.
$EuSi_{6-x}Ga_x$	8 GPa, 1500 K	$EuGa_2Ge_4$	147
Ba_6Si_{25}	1 GPa, 1070 K	$Ba_6In_4Ge_{21}$	148
Ba_8Si_{46}	3 GPa, 1070 K	K_4Si_{23}	149
$Ba_{8-\delta}Si_{46}$	3 GPa, 1070 K	K_4Si_{23}	150
$BaSi_{6-x}$	12 GPa, 1070 K		151
$Ba_{8-\delta}Si_{46-x}Ge_x$	3 GPa, 1070 K	K_4Si_{23}	152
$Ba_6Ge_{25-x}Si_x$	1 GPa, 800 K	$Ba_6Ge_{23}In_2$	153
$Ba_{8-x}Eu_xGe_{43}$	1 GPa, 800 K	Ba_8Ge_{43}	154
$SrGe_{6-\delta}$	5 GPa, 1470 K	$SrGe_{6-\delta}$	155
$LaGe_5$	5 GPa, 1470 K	$LaGe_5$	156

Table 5. High-pressure phase transitions or syntheses of intermetallic compounds with 1 : 3 composition.

Compound of type A_3B	Structure type low-pressure phase	Transition or synthesis conditions	Structure type high-pressure phase	Lit.
V_3Al	Cr_3Si	2 GPa, 1770 K	*Tetragonal*	157
V_3Al		4 GPa, 1900 K	*Hexagonal*	157
V_3Al		2.5 GPa, 1170 K	*bcc*	157
$OsGa_3$		7.7 GPa, 570 K	β-$ReGa_3$	158
Nb_3In		3.2 GPa, 1173 K	Cr_3Si	159
$CeGe_3$		5 GPa, 1873 K	Cu_3Au	160
Nb_3Ge		2 GPa, 1073 K	Cr_3Si	161
$PtSn_3$		7.0 GPa, 1173 K	*Cubic*	162
$LuPb_3$		6.7–8.8 GPa, 973 K	Cu_3Au	163
Nb_3Pb		2 GPa, 1073 K	Cr_3Si	161
Li_3As	Na_3As	4.5 GPa	BiF_3	118
Na_3As	Cu_3P	3.6 GPa	BiF_3	164
Na_3Sb	Na_3As	1.8 GPa	BiF_3	118
Mn_3Sb		6.2 GPa,1273 K	Cu_3Au	165
Na_3Bi	Na_3As	1 GPa	BiF_3	118
Nb_3Bi		3.5 GPa, 1273 K	Cr_3Si	159
Yb_3Co		7.7 GPa, heating	Fe_3C	166
Yb_3Ni		7.7 GPa, heating	Al_3Ni	166
K_3Ag		6.4 GPa	BiF_3	54

High-pressure synthesis of clathrates

The finding of superconductivity in some intermetallic clathrates prompted intense interest in synthesis and physical properties of these compounds. Their atomic arrangement is characterized by an anionic framework of a majority component with cage-like voids centred by cations. Several clathrates are accessible by high-pressure synthesis, *e.g.*, Ba_6Si_{25}, Ba_8Si_{46}, $Ba_{8-x}Si_{46-y}Ge_y$, and $Ba_{8-x}Eu_xGe_{43}\square_3$ (Table 4). It was noted that high-pressure treatment is necessary for the preparation of silicides like Ba_6Si_{25} and Ba_8Si_{46} while the corresponding germanium compounds can be synthesized at ambient pressure. Taking into account the small size difference between silicium and germanium, it remains to be investigated whether the formation of Si clathrates by compression can be attributed to a thermodynamic stabilization of the clathrate relative to competing phases. Alternatively, the large melting point difference of the two elements and the higher synthesis temperatures required for the silicon compounds certainly causes elevated partial pressures of low-boiling components which may demand high pressures for compensation.

Summary

The knowledge concerning the formation of high-pressure phases of intermetallic compounds is still rather imcomplete. The large number of different structure types and compositions other than 1 : 1 or 1 : 2 (Tables 5 and 6) impedes the clear recognition of patterns in this group. Systematic investigations of compound series are available for some strongly polar Zintl-type phases and a subset of AlB_2-type compounds. However, despite some empirical concepts to predict the effect of pressure application, a clear picture of the structural phase transitions has not evolved yet. This is partly due to the fact that only a few pressure-induced structural changes have been investigated by quantum mechanical calculations of the total energy. The hitherto available experimental data evidence a rich crystal chemistry of Zintl phases upon compression and the stability of most AlB_2-type atomic patterns at reduced volumes. The large number of synthesized Laves phases underlines their description as a dense-packing of two atom types and justifies the expectation that more representatives will form at high-pressure conditions.

Table 6. High-pressure syntheses of intermetallic compounds with various compositions.

Compound	Synthesis conditions	Structure type	Lit.
Pd_8Al_{21}	4 GPa, 1673 K	Pt_8Al_{21}	167
Ta_6Ga_5	7.7 GPa, 2273 K	Ti_6Sn_5	168
Mo_5Ga_3	7.7 GPa, 873 K	W_5Si_3	169
Mo_5Ga_3	7.7 GPa, 623 K	Cr_5B_3	169
Mo_6Ga_3	7.7 GPa, 623 K	Ti_6Sn_5	169
Mo_6Ga_7	7.7 GPa, 873 K	*Cubic*	169
W_2Ga_5	7.7 GPa, 573 K	Mn_2Hg_5	170
Co_2Si_3	4 GPa, 773 K	Ru_2Sn_3	171
W_5Ge_3	7.7 GPa, 873 K	W_5Si_3	172
W_5Ge_3	7.7 GPa, 873 K	Cr_5B_3	172
Mn_3Ge_5	4 GPa, 1073 K	$Mn_{11}Si_{19}$	173
$MnGe_4$	5.5 GPa, 873 K	*Tetragonal*	174
Re_4Ge_7	4 GPa, 973 K	Mn_4Si_7	171
$CoGe_4$	6 GPa, 873 K	Cubic	174
$RhGe_4$	2.5 GPa, 1000 K	$IrGe_4$	175
Mg_9Sn_5	5 GPa, 1673 K	Mg_9Sn_5	112
$IrSn_4$	6.0 GPa, 1173 K	$PtSn_4$	175
Yb_6Mn_{23}	7.7 GPa, 1470 K	Th_6Mn_{23}	130
Yb_4Mn_3	7.7 GPa, 1620 K	Ho_4Co_3	130
Yb_2Mn_{17}	7.7 GPa, 1470 K	Th_2Ni_{17}	130
Yb_2Ni_7	7.7 GPa, heating	Gd_2Ni_7	166
Tb_6Cu_{23}	7.7 GPa	Th_6Mn_{23}	176
Dy_6Cu_{23}	7.7 GPa	Th_6Mn_{23}	176
Yb_6Cu_{23}	7.7 GPa	Th_6Mn_{23}	176
Lu_6Cu_{23}	7.7 GPa	Th_6Mn_{23}	176
Ca_3Au_4	75 atm of N_2	Pu_3Pd_4	177

Acknowledgment. The authors wish to express their gratitude to Daniel Grüner, Frank R. Wagner and Karl Syassen for valuable discussions.

References

[1] Hume-Rothery, W.: J. Inst. Metals **35** (1925) 209–212.
[2] Zintl, E.; Kaiser, H.: Über die Fähigkeit der Elemente zur Bildung negativer Ionen. Z. Anorg. Allg. Chem. **211** (1933) 113–131.
[3] Zintl, E.: Intermetallische Verbindungen. Angew. Chem. **52** (1939) 16.
[4] Laves, F.: Kristallographie der Legierungen. Naturwissenschaften **27** (1939) 65–73.
[5] Schäfer, H.; Eisenmann, B.; Müller, W.: Zintl-Phasen: Übergangsformen zwischen Metall- und Ionenbindung. Angew. Chem. **85** (1973) 742–760; Zintl-Phases: Transitions between metallic and ionic bonding. Angew. Chem. Int. Ed. **12** (1973) 694–712.
[6] Pearson, W. B.: The stability of metallic phases and structures – Phases with the AlB_2 and related structures. Proc. R. Soc. Lond. A**365** (1979) 523–535.
[7] Simon, A.: Intermetallische Verbindungen und die Verwendung von Atomradien zu ihrer Beschreibung. Angew. Chem. **95** (1983) 94–113; Intermetallic compounds and the use of atomic radii in their description. Angew. Chem. Int. Ed. **22** (1983) 95–113.
[8] Nesper, R.: Structure and chemical bonding in Zintl-phases containing lithium. Prog. Sol. St. Chem. **20** (1990) 1–45.
[9] Nesper, R.: Chemische Bindungen – intermetallische Verbindungen. Angew. Chem. **103** (1991) 805–834; Bonding patterns in intermetallic compounds. Angew. Chem. Int. Ed. **30** (1991) 789–817.
[10] Zunger, A.: Systematization of the stable structure of all AB-type binary compounds: A pseudopotential orbital-radii approach. Phys. Rev. B**22** (1980) 5839–5872.
[11] Villars, P.; Mathis, K.; Hullinger, F.: Enviroment classification and structural stability maps. In: The structures of binary compounds. (Eds. F. R. de Boer; D. G. Pettifor). North Holland 1989.
[12] Sommer, A. H.: Alloys of gold with alkali metals. Nature **152** (1943) 215.
[13] Spicer, W. E.; Sommer, A. H.; White, J. G.: Studies of the semiconducting properties of the compound CsAu. Phys. Rev. **115** (1959) 57–62.
[14] Kienast, G.; Verma, J.; Klemm, W.: Das Verhalten der Alkalimetalle zu Kupfer, Silber und Gold. Z. Anorg. Allg. Chem. **310** (1961) 143–169.
[15] Zachwieja, U.: Single-crystal growth and structure refinement of RbAu and CsAu. Z. Anorg. Allg. Chem. **619** (1993) 1095–1097.

[16] Neuhaus, A.: Synthese, Strukturverhalten und Valenzzustände der anorganischen Materie im Bereich hoher und höchster Drucke. Chimia **18** (1964) 93–103.
[17] Schwarz, U.; Jepsen, O.; Syassen, K.: Electronic structure and bonding in the *Cmca* phase of Si and Cs. Solid State Commun. **113** (2000) 643–648.
[18] Christensen, N. E.; Novikov, D. L.; Methfessel, M.: The intermediate high-pressure phase of silicon. Solid State Commun. **110** (1999) 615–619.
[19] Beister, H. J.; Strössner, K.; Syassen, K.: Rhombohedral to simple-cubic phase transition in arsenic under pressure. Phys. Rev. B**41** (1990) 5535–5543.
[20] Moruzzi, V. L.; Janak, V. F.; Williams, A. R.: Calculated electronic properties of metals. Pergamon 1978.
[21] Koepernik, K.; Eschrig, H.: Full-potential nonorthogonal local-orbital minimum-basis band-structure scheme. Phys. Rev. B**59** (1999) 1743–1757.
[22] Becke, A. D.; Edgecombe, K. E.: A simple measure of electron localization in atomic and molecular systems. J. Chem. Phys. **92** (1990) 5397–5403.
[23] Savin, A.; Jepsen, O.; Flad, J.; Andersen, O. K.; Preuss, H.; von Schnering, H. G.: Die Elektronenlokalisierung in den Festkörperstrukturen der Elemente: Die Diamantstruktur. Angew. Chem. **104** (1992) 186–188; Electron localization in solid-state structures of the elements: The diamond structure. Angew. Chem. Int. Ed. **31** (1992) 187–188.
[24] Kohout, M.: A measure of electron localizability. Int. J. of Quant. Chem. **97** (2004) 651–658.
[25] Perdew, J. P.; Wang, Y.: Accurate and simple analytic representation of the electron-gas correlation energy. Phys. Rev. B**45** (1992) 13244–13249.
[26] Eschrig, H.: Optimized LCAO Method and the Electronic Structure of Extended Systems. Springer, Berlin, 1989.
[27] Ormeci, A.; Rosner, H.; Wagner, F. R.; Kohout, M.; Grin, Yu.: Electron localization function in full-potential representation for crystalline materials. J. Phys. Chem. A**110** (2006) 1100–1105.
[28] von Schnering, H. G.; Nesper, R.: Die natürliche Anpassung von chemischen Strukturen an gekrümmte Flächen. Angew. Chemie **99** (1987) 1097–1119; How nature adopts chemical structures to curved surfaces. Angew. Chemie Int. Ed. Engl. **26** (1987) 1059–1080.
[29] Andersen, O. K.; Jepsen, O.: unpublished results.
[30] Brauer, G.; Mitius, A.: Crystal structure of Thorium silicides $ThSi_2$. Z. Anorg. Allg. Chem. **249** (1942) 325–339.
[31] Wagner, F.; Kohout, M.; Grin, Yu.: ELF development: d–d interactions. Scientific report, Max-Planck-Institut für Chemische Physik fester Stoffe (2000) 128–132.
[32] Hanfland, M.; Syassen, K.; Christensen, N. E.; Novikov, D. L.: New high-pressure phases of lithium. Nature **408** (2000) 174–178.
[33] Hanfland, M.; Loa, I.; Syassen, K.: Sodium under pressure: *bcc* to *fcc* structural transition and pressure-volume relation to 100 GPa. Phys. Rev. B**65** (2002) 184109.
[34] Sternheimer, R. M.: On the compressibility of metallic cesium. Phys. Rev. **75** (1949) 888–889.
[35] Ahuja, R.; Eriksson, O.; Wills, J. M.; Johannson, B.: Theoretical confirmation of the high pressure simple cubic phase in calcium. Phys. Rev. Lett. **75** (1995) 3473–3476.
[36] Zheng, W.-S.; Heine, V.; Jepsen, O.: The structure of barium in the hexagonal close-packed phase under high pressure. J. Phys.: Condens. Matter **9** (1997) 3489–3502.
[37] McMahan, A. K.; Skriver, H. L.; Johansson, B.: The s–d transition in compressed lanthanum. Phys. Rev. B**23** (1981) 5016–5029.
[38] Takemura, K.; Minomura, S.; Shimomura, O.: X-ray diffraction study of electronic-transitions in cesium under high-pressure. Phys. Rev. Lett. **49** (1982) 1772–1775.
[39] Schwarz, U.; Takemura, K.; Hanfland, M.; Syassen, K.: Crystal structure of cesium-V. Phys. Rev. Lett. **81** (1998) 2711–2714.
[40] Schwarz, U.; Grzechnik, A.; Syassen, K.; Loa, I.; Hanfland, M.: Rubidium-IV: A high pressure phase with complex crystal structure. Phys. Rev. Lett. **83** (1999) 4085–4088.
[41] McMahon, M. I.; Nelmes, R. J.: Chain "melting" in the composite Rb-IV structure. Phys. Rev. Lett. **93** (2004) 055501.
[42] Nelmes, R.; Allan, D. R.; McMahon, M. I.; Belmonte, S. A.: Self-hosting incommensurate structure of barium IV. Phys. Rev. Lett. **83** (1999) 4081–4084.
[43] McMahon, M.; Nelmes, R.: Incommensurate crystal structures in the elements at high pressure. Z. Kristallogr. **219** (2004) 742–748.
[44] Schwarz, U.: Metallic high-pressure modifications of main group elements. Z. Kristallogr. **219** (2004) 376–390.
[45] Jamieson, J. C.: Crystal structures of titanium, zirconium, and hafnium at high pressures. Science **140** (1963) 72.
[46] Jayaraman, A.; Clerment, W.; Kennedy, G. C.: Solid-Solid transitions in titanium and zirconium at high pressures. Phys. Rev. **131** (1963) 644.
[47] Sikka, S. K.; Vohra, Y. K.; Chidambaram, R.: Omega-phases in materials. Progr. Mater. Sci. **27** (1982) 245–310.
[48] Xia, H.; Parthasarathy, G.; Luo, H.; Vohra, Y. K.; Ruoff, A. L.: Crystal structures of group IVa metals at ultrahigh pressures. Phys. Rev. B**42** (1990) 6736–6738.
[49] Ahuja, R.; Wills, J. M.; Johansson, B.; Erikson, O.: Crystal structures of Ti, Zr, and Hf under compression: Theory. Phys. Rev. B**48** (1993) 16269–16279 and references therein.
[50] Kohout, M.: Die Elektronen-Lokalisierungs-Funktion und ionische Bindung. Thesis, Universität Stuttgart 1999.
[51] Kohout, M.; Wagner, F. R.; Grin, Yu.: Electron localization function for transition metal compounds. Theor. Chem. Acc. **108** (2002) 150–156.
[52] Mulliken, R. S.: Electronic population analysis on LCAO-MO molecular wave functions. I. J. Chem. Phys. **23** (1955) 1833–1840.
[53] Mulliken, R. S.: Electronic population analysis on LCAO-MO molecular wave functions. II. Overlap populations, bond orders, and covalent bond energies. J. Chem. Phys. **23** (1955) 1841–1846.
[54] Atou, T.; Hasegawa, M.; Parker, L. J.; Badding, J. V.: Unusual chemical behaviour for potassium under pressure: Potassium silver compounds. J. Am. Chem. Soc. **118** (1996) 12104–12108.
[55] Iwasaki, H.: X-ray study of the compression of the alloy MgIn. Acta Metall. **26** (1978) 647–650.
[56] Iwasaki, H.: An X-ray diffraction study of lattice compression of the L 1_o-type intermetallic phase PdZn. Acta Crystallogr. A **36** (1980) 299–303.
[57] Iwasaki, H.; Okada, M.: The γ-brass structure at high pressure. Acta Crystallogr. B**36** (1980) 1762–1765.
[58] Wood, I. G.; David, W. I. F.; Hull, S.; Price, G. D.: A high-pressure study of epsilon-FeSi, between 0 and 8.5 GPa, by time-of-flight neutron powder diffraction. J. Appl. Cryst. **29** (1996) 215–218.
[59] Wood, I. G; Chaplin, T. D.; David, W. I. F.; Hull, S.; Price, G. D.; Street, J. N.: Compressibility of FeSi between 0 and 9 GPa, determined by high-pressure time-of-flight neutron powder diffraction. J. Phys.: Condens. Matter **7** (1995) L475–L479.
[60] Knittle, E.; Williams, Q.: Static compression of ε-FeSi and an evaluation of reduced silicon as a deep earth constituent. Geophys. Res. Lett. **22** (1995) 445–448.
[61] Larsson, A. K.; Haeberlein, M.; Lidin, S.; Schwarz, U.: Single crystal structure refinement and high-pressure properties of CoSn. J. Alloys Comp. **240** (1996) 79–84.
[62] Chandra Shekar, N. V.; Sahu, P. Ch.; Yousuf, M.; Govinda Rajan, K.; Rajagoplan, M.: Structural stability and compressibility behaviour of dialuminides of cerium and gadolinium under high pressure. Solid State Commun. **111** (1999) 529–533.
[63] Kurisu, M.: Structural and magnetic properties of RAg (R = La, Ce, Pr and Nd) at hydrostatic pressures up to 37 kbar. J. Phys. Soc. Jpn. **56** (1987) 4064–4074, and references therein.
[64] Büchler, H.; Range, K.-J.: Hochdruck-Hochtemperatursynthese und Kristallstruktur von $Al_{11}Au_6$ und AlAu. J. Less Common Metals **160** (1990) 143–152.
[65] Büchler, H.; Range, K.-J.: Hochdrucksynthese und Kristallstruktur von Al_3Au_8. J. Less Common Metals **154** (1989) 251–260.
[66] Büchler, H.; Range, K.-J.: Zur Kenntnis des β-Mangan-Typs: Hochdrucksynthese uns Strukturverfeinerung von $AlAu_4$. J. Less Common Metals **161** (1990) 347–354.
[67] Christensen, N. E.: Structural phase-stability of B2 and B32 intermetallic compounds. Phys. Rev. B**32** (1985) 207–228.
[68] Stein, F.; Palm, M.; Sauthoff, G.: Structure and stability of Laves phases. Part I. Critical assessment of factors controlling Laves phase stability. Intermetallics **12** (2004) 713–720.

[69] Loubeyre, P.; Jean-Louis, M.; LeToullec, R.: High pressure measurements of the He−Ne binary phase diagram at 296 K: Evidence for the stability of a stoichiometric $Ne(He)_2$ solid. Phys. Rev. Lett. **70** (1993) 178–181.

[70] Schwarz, U.; Bräuninger, S.; Syassen, K.; Kniep, R.: Pressure-induced phase transformation of LiIn and LiCd: From NaTl-type phases to β-brass-type alloys. J. Solid State Chem. **137** (1998) 104–111.

[71] Evers, J.; Oehlinger, G.: After more than 60 years, a new NaTl type Zintl phase: KTl at high pressure. Inorg. Chem. **39** (2000) 628–629.

[72] Evers, J.; Oehlinger, G.; Sextl, G.: LiSi, a unique Zintl phase – although stable, it long evaded synthesis. Eur. J. Sol. State Inorg. **34** (1997) 773–784.

[73] Evers, J.; Oehlinger, G.; Sextl, G.; Weiß, A.: Hochdruckphasen von KSi, KGe, RbSi, RbGe, CsSi und CsGe im NaPb-Typ. Angew. Chem. **96** (1984) 512–513; High-pressure phases of KSi, KGe, RbSi, RbGe, CsSi and CsGe with the NaPb-type structure. Angew. Chem. Int. Ed. **23** (1984) 528–529.

[74] Dobson, D. P.; Vocaldo, L.; Wood, I. G.: A new high-pressure phase of FeSi. American Mineralogist **87** (2002) 784–787.

[75] Evers, J.; Oehlinger, G.; Sextl, G.; Becker, H. O.: Hochdruck-LiGe mit Schichten aus zwei- und vierbindigen Germaniumatomen. Angew. Chem. **99** (1987) 69–71; High-pressure LiGe with layers containing 2-coordinate and 4-coordinate germanium atoms. Angew. Chem. Int. Ed. **26** (1987) 76–78.

[76] Evers, J.; Oehlinger, G.: Isolierte hexagonale Kanäle aus dreibindigen Ge^--Ionen in Hochdruck-LiGe. Angew. Chem. **113** (2001) 1085–1088; Isolated hexagonal channels built up by three-connected Ge^--ions in LiGe at high pressure. Angew. Chem. Int. Ed. **40** (2001) 1050–1053.

[77] Evers, J.; Oehlinger, G.; Sextl, G.; Weiß, A.: NaGe bei hohen Drücken auch im NaPb-Typ. Angew. Chem. **97** (1985) 499–500; NaGe: High-pressure formation of the NaPb-type structure. Angew. Chem.. Int. Ed. **24** (1985) 500–501.

[78] Takizawa, H.; Sato, T.; Endo, T.; Shimada, M.: High-pressure synthesis and electrical and magnetic properties of MnGe and CoGe with cubic B20 structure. J. Solid State Chem. **73** (1988) 40–46.

[79] Larchev, V. I.; Popova, S. V.: The polymorphism of transition-metal monogermanides at high-pressures and temperatures. J. Less Common Metals **87** (1982) 53–57.

[80] Beck, H. P.; Lederer, G.: Thermal dilatation and high-pressure behavior of Zinl phases CaSn and BaSn. Z. Anorg. Allg. Chem. **619** (1993) 897–900.

[81] Adachi, T.; Shirotani, I.; Hayashi, J.; Shimomura, O.: Phase transitions of lanthanide monophosphides with NaCl-type structure at high pressures. Physics Letters A**250** (1998) 389–393.

[82] Vedel, I.; Redone, A. M.; Rossat Mignod, J.; Vogt, O.; Leger, J. M.: Electronic and crystallographic transitions induced by pressure in CeP. J. Phys. C: Solid State Physics **20** (1987) 3439–3444.

[83] Hayashi, J.; Shirotani, I.; Adachi, T.; Shimomura, O.; Kikegawa, T.: Phase transitions of YbX (X = P, As and Sb) with a NaCl-type structure at high pressures. Philosophical Magazine **84** (2004) 3663–3670.

[84] Leger, J. M.; Ravot, D.; Rossar-Mignot, J.: Volume behaviour of CeSb and LaSb up to 25 GPa. J. Phys. C **17** (1984) 4935–4943.

[85] Hayashi, J.; Shirotani, I.; Tanaka, Y.; Adachi, T.; Shimomura, O.; Kikegawa, T.: Phase transitions of LnSb (Ln = lanthanide) with NaCl-type structure at high pressures. Solid State Commun. **114** (2000) 561–565.

[86] Leger, J. M.; Oki, K.; Rossat-Mignod, J.; Vogot, O.: Structural transition and volume compression of CeBi up to 20 GPa. J. Phys. **46** (1985) 889–894.

[87] Meresse, Y.; Heathman, S.; Rijkeboer, C.; Rebizant, J.: High pressure behaviour of PuBi studied by X-ray diffraction. J. Alloys Comp. **284** (1999) 65–69.

[88] Tang, J.; Kosaka, T.; Matsumura, T.; Matsumoto, T.; Suzuki, T.: The valence state of TmTe at high pressure. Solid State Commun. **100** (1996) 571–574.

[89] Heathman, S.; Le Bihan, T.; Darracq, S.; Abraham, C.; De Ridder, D. J. A.; Benedict, U.; Mattenberger, K.; Vogt, O.: High-pressure behavior of TmTe and EuO. J. Alloys Comp. **230** (1995) 89–93.

[90] Usha Devi, S.; Singh, A. K: Pressure induced structural transformation in thulium monotelluride. Solid State Commun. **52** (1984) 303–305.

[91] Degtyarova, V. F.; Porsch, F.; Khasanov, S. S.; Shekhtman, V. S.; Holzapfel, W. B.: Effect of pressure on structural properties of intermetallic LnM lanthanide compounds. J. Alloys Comp. **246** (1997) 248–255.

[92] Iwasaki, H.; Fujimura, T.; Ichikawa, M.; Endo, S.; Wakatsuki, M. J.: Pressure-induced phase transformation in AgZn. J. Phys. Chem. Solids **46** (1985) 462–468.

[93] Popova, S. V.; Fomicheva, L. N.; Putro, V. G.: Neorganicheskij Materialy **16** (1980) 1065–1068; High-pressure phases in the scandium−gallium system. Inorg. Materials **16** (1980) 1065–1068.

[94] Schekar, N. V. C.; Subramanian, N.; Kumar, N. R. S.; Sahu P. C.: Phase transformation in $CeGa_2$ under high pressure. phys. stat. sol. b **241** (2004) 2893–2897.

[95] Schwarz, U., Bräuninger, S., Grin, Yu., Syassen, K.; Hanfland, M.: Structural phase transition of $HoGa_2$ at high pressure. J. Alloys Comp. **268** (1998) 161–165.

[96] Schwarz, U.; Bräuninger, S.; Grin, Yu.; Syassen, K.: Structural phase transition of $TmGa_2$ at high pressure. J. Alloys Comp. **245** (1996) 23–29; J. Alloys Comp. **256** (1997) 279.

[97] Schwarz, U.; Giedigkeit, R.; Niewa, R.; Schmidt, M.; Schnelle, W.; Cardoso, R.; Hanfland, M.; Hu, Z.; Klementiev, K.; Grin, Yu.: Pressure-induced oxidation state change of ytterbium in $YbGa_2$. Z. Anorg. Allg. Chem. **627** (2001) 2249–2256.

[98] Popova, S. V.; Fomicheva, L. N.; Neorganicheskij Materialy **18** (1982) 205–208; New phases in Re−Ga and Os−Ga systems, obtained at a high pressure. Inorg. Materials **18** (1982) 251–255.

[99] Schwarz, U.; Bräuninger, S.; Burkhardt, U.; Syassen, K.; Hanfland, M.: Structural phase transition of $GdGa_2$ at high pressure. Z. Kristallogr. **216** (2001) 331–336.

[100] Godwal, B. K.; Jayaraman, A.; Meenakashi, S.; Rao, R. S.; Sikka, S. K.; Vijyyakumar, V.: Electronic topological and structural transition in $AuIn_2$ under pressure. Phys. Rev. B**57** (1998) 773–776.

[101] Cannon, P.; Conlin, E. T.: Magnesium compounds – new dense phase. Science **145** (1964) 487–489.

[102] Dyuzheva, T. I.; Kabalkina, S. S.; Vereshchagin, L. F.: Dokl. Akad. Nauk SSSR **228** (1976) 1073–1075; Polymorphism of intermetallic compounds Mg_2Si and Mg_2Ge under high-pressure. Soviet Physics Doklady **21** (1976) 342–344.

[103] Evers, J.; Oehlinger, G.; Weiss, A. J.: Effect of pressure on the structure of divalent metal disilicides MSi_2 (M = Ca, Eu, Sr). J. Solid State Chem. **20** (1977) 173–181.

[104] Bordet, P.; Affronte, M.; Sanifilippo, S.; Núñez-Regueiro, M.; Olcese, G. L.; Palenzona, A.; LeFloch, S.; Levy, D.; Hanfland, M.: Structural phase transition in $CaSi_2$ under high pressure. Phys. Rev. B**62** (2000) 11392–11397.

[105] Evers, J.: Transformation of 3-connected silicon in $BaSi_2$. J. Solid State Chem. **32** (1980) 77–86.

[106] Evers, J.; Oehlinger, G.; Weiss, A.: Crystal structure of $SrGe_2$ at high pressure. Z. Naturforsch. **34b** (1979) 524.

[107] Evers, J.; Oehlinger, G.; Weiss, A.: Structural refinement of the high-pressure high-temperature phase of $BaGe_2$. Z. Naturforsch. **35b** (1980) 397–398.

[108] Agoshkov, V. M.; Gorbatenkov, V. D.; Popova, S. V.; Fomicheva, L. N.: Crystalliztion of $MoGe_2$ and WGe_2 at high-pressure and some properties of these phases. J. Less Common Metals **17** (1981) 1523–1526.

[109] Agoshkov, V. M.; Gorbatenkov, V. D.; Popova, S. V.; Fomicheva, L. N.: Formation conditions and certain properties of $MoGe_2$ and WGe_2 phases obtained at high-presure. Inorg. Materials **17** (1981) 1523–1526.

[110] Popova, S. V.; Fomicheva, L. N.: Synthesis of tungsten germanides at high-pressure. Inorg. Materials **14** (1978) 533–535.

[111] Takizawa, H.; Uheda, K.; Endo, T.: $NiGe_2$: A new intermetallic compound synthesized under high-pressure. J. Alloys Comp. **305** (2000) 306–310.

[112] Range, K.-J.; Grosch, H. G.; Andratschke, M.: Studies on AB_2-type intermetallic compounds. Part V[1]. The crystal structure of Mg_9Sn_5, a supposed high-pressure modification of Mg_2Sn. J. Alloys Comp. **244** (1996) 170–174.

[113] Larchev, V. I.; Popova, S. V.: New phases in the system Pt−Sn at high pressure. Inorg. Materials **20** (1984) 693–695.
[114] Alekseev, E. S.; Popova, S. V.; Larchev, V. I.: High-pressure phase $PtPb_2$ – Synthesis, structure and properties. J. Alloys Comp. **176** (1991) 1–6.
[115] Eatough, N. L.; Hall, T. H.: High-pressure synthesis of rare earth diantimonides. Inorg. Chem. **8** (1969) 1439–1445.
[116] Takizawa, H.; Uheda, K.; Endo, T.: A new ferromagnetic polymorph of $CrSb_2$ synthesized under high pressure. J. Alloys Comp. **287** (1999) 145–149.
[117] Takizawa, H.; Uheda, K.; Endo, T.: A new high-pressure polymorph of $NiSb_2$. Intermetallics **8** (2000) 1399–1403.
[118] Beister, H.-J.; Klein, J.; Schewe, I.; Syassen, K.: Structural phase transitions of alkali metal pnictides and chalcogenides under pressure. High Pressure Research **7** (1991) 91–95.
[119] Lindbaum, A.; Heathman, S.; Kresse, G.; Rotter, M.; Gratz, E.; Schneidewind, A.; Behr, G.; Litfin, K.; Le Bihan, T.; Svoboda, P.: Structural stability of $LaCu_2$ and YCu_2 studied by high-pressure X-ray diffraction and ab initio total energy calculations. J. Phys. Condens. Matter **12** (2000) 3219–3228.
[120] Beister, H.-J.; Syassen, K.; Deiseroth, H.-J.; Tolstede, D.: Pressure-induced phase transition of the alkali metal amalgam KHg_2. Z. Naturforsch. **48b** (1993) 11–14.
[121] Ebner, M. A.; Range, K.-J.: Studies on AB_2-type intermetallic compounds, II. High-pressure synthesis and crystal structure of $MgEr_2$ and $MgTb_2$. J. Alloys Comp. **236** (1996) 34–37.
[122] Ebner, M. A.; Range, K.-J.: Studies on AB_2-type intermetallic compounds, III. High-pressure synthesis and single-crystal structure refinement of the Laves-Friauf phases of $HoMg_2$, $TmMg_2$ and $YbMg_2$. J. Alloys Comp. **236** (1996) 50–57.
[123] Gordier, G.; Czech, E.; Schäfer, H.: Über eine Hochdruckmodifikation des $SrAl_2$. Z. Naturforsch. **37b** (1982) 1442–1445.
[124] Gordier, G.; Czech, E.; Schäfer, H.; Zur Kenntnis der Hochdruckphase $BaAl_2$. Z. Naturforsch. **39b** (1984) 421–423.
[125] Godwal, B. K.; Vijaykumar, V.; Sikka, S. K.; Chidambaram, R.: Pressure-induced AlB_2 to $MgCu_2$-type structural transition in $ThAl_2$. J. Phys. F: Met. Phys. **16** (1986) 1415–1418.
[126] Sachu, P. Ch.; Shekar, C.; Subramanian, N.: Crystal structure of UAl_2 above 10 GPa at 300 K. J. Alloys Comp. **223** (1995) 49–52.
[127] Hupperts, H.; Kotzuba, G.; Hoffmann, R.-D.; Pöttgen, R.: Decomposition of EuPdIn and EuPtIn at high temperature and high pressure-formation of the hexagonal Laves phases $EuPd_{0.72}In_{1.28}$ and $EuPt_{0.56}In_{1.44}$. J. Solid State Chem. **169** (2002) 155–159.
[128] Eatough, N. L.; Hall, H. T.: High-pressure synthesis of rare earth dimanganese compounds with the $MgZn_2$ (Laves) structure. Inorg. Chem. **11** (1972) 2608–2609.
[129] Nakamura, H.; Moriwaki, M.; Shiga, M.; Inoue, K.; Nakamura, Y.; Tsvyashchenko, A. V.; Fomicheva, L. N.: ^{55}Mn nuclear magnetic resonance study of high-pressure synthesized hexagonal $DyMn_2$, $TbMn_2$ and $GdMn_2$. J. Magnetism and Magnetic Materials **150** (1995) L137–L142.
[130] Tsvyaschchenko, A. V.; Popova, S. V.: High pressure phases in the Mn−Yb system. J. Less Common Metals **90** (1983) 211–215.
[131] Cannon, J. F.; Robertson, D. L.; Hall, H. T.: Synthesis of lanthanide-iron Laves phases at high pressures and temperatures. Mat. Res. Bull. **7** (1972) 5–12.
[132] Lindbaum, A.; Heathman, S.; Le Bihan, T.; Rogl P.: Pressure-induced orthorhombic distortion of UMn_2. J. Alloys Comp. **298** (2000) 177–180.
[133] Tsvyashchenko, A. V.; Popova, S. V.: New phases melt quenched under high-pressure in *R*-Fe systems (R = Pr, Sm, Dy, Tb, Ho, Er, Tm, Yb, Lu). J. Less Comm Metals **108** (1985) 115–121.
[134] Zhao, X.; Li, J.; Liu, S.; Ji, S.; Jia, K.: Magnetic properties and thermal stability of $PrFe_2$ compound. J. Alloys Comp. **258** (1997) 39–41.
[135] Notsu, Y.; Endo S.; Ono, F.; Kohmoto, O.; Uchida, T.; Mori, T.: High pressure synthesis and magnetostrictive measurement of Laves phase $Pr_{1-x}R_xFe_2$ (R = Ce, Nd). Jpn. J. Appl. Phys. **32** (1993) 327–328.
[136] Meyer, C.; Srour, B.; Gros, Y.; Hartmann-Boutron, F.; Capponi, J. J.: Synthesis, magnetic properties and ^{57}Fe Mössbauer study of the Laves phase compound $YbFe_2$. J. Physique **38** (1977) 1449–1455.
[137] Tsyvashchenko, A. V.; Makhotkin, V. E.; Fradkov, V. A.; Kuznetsov, V. N.: Synthesis and magnetic-properties of cubic Laves phase-compounds YFeCu, GdFeCu and $Yb(Fe_{1-x}Cu_x)_2$. J. Less Common Metals **118** (1986) 173–181.
[138] Cannon, J. F.; Robertson, D. L.; Hall, H. T.: The effect of high pressure on the formation of LRu_2 and LOs_2 (L = Lanthanide) compounds. J. Less Common Metals **29** (1972) 141–146.
[139] Cannon, J. F.; Robertson, D. L.; Hall, H. T.: The effect of high pressure on the crystal structure of $LaOs_2$ and $CeOs_2$. J. Less Common Metals **31** (1973) 174–176.
[140] Tsvyashchenko, A. V.; Fomicheva, L. N.; Magnitskaya, M. V.; Sidirorv, V. A.; Kuznetsov, A. V.; Eremenko, D. V.; Trofimov, V. N.: Pis'Ma V Zhurnal Eksperimental'Noi i Teoreticheskoi Fiziki **68** (1998) 864; New ferromagnetic compound $CaCo_2$ (C15) synthesized at high pressure. JETP Letters **68** (1998) 908–914.
[141] Tsvyashchenko, A. V.; Fomicheva, L. N.; Magnitskaya, M. V.; Sidirorv, V. A.; Shirani, E. N.; Kuznetsov, A. V.; Eremenko, D. V.; Trofimov, V. N.: Magnetism of Ca-3*d* metal Laves-phase compounds synthesized at high pressure. The Physics of Metals and Metallography **93** (2002) 59–63.
[142] Robertson, D. L.; Cannon, J. F.; Hall, H. T.: High-pressure and high-temperature synthesis of $LaCo_2$. Mat. Res. Bull. **7** (1972) 977.
[143] Hasegawa, M.; Atou, T.; Badding, J. V.: High-pressure synthesis of an alkali metal-transition metal Laves phase: KAg_2. J. Solid State Chem. **130** (1997) 311–315.
[144] Range, K.-J.; Rau, F.; Klement, U.: Potassium Digold, KAu_2. Acta Crystallogr. C**44** (1988) 1485–1486.
[145] Range, K.-J.; Rau, F.; Klement, U.: Sodium Diplatinum. Acta Crystallogr. C**45** (1989) 1069–1070.
[146] Liu, X.; Rau, F.; Breu, J.; Range, K.-J.: Studies on AB_2-type intermetallic compounds, IV. High-pressure synthesis and crystal structure of scandium dizinc $ScZn_2$. J. Alloys Comp. **243** (1996) L5–L7.
[147] Wosylus, A.; Prots, Yu.; Burkhardt, U.; Schnelle, W.; Schwarz, U.; Grin, Yu.: Breaking the Zintl rule: high-pressure synthesis of binary $EuSi_6$ and its ternary derivative $EuSi_{6-x}Ga_x$ ($0 \le x \le 0.6$). Solid State Science, in press.
[148] Fukuoka, H.; Ueno, K.; Yamanaka S.: High-pressure synthesis and structure of a new silicon clathrate $Ba_{24}Si_{100}$. J. Organomet. Chem. **611** (2000) 543–546.
[149] Yamanaka, S.; Enishi, E.; Fukuoka, H.; Yasukawa, M.: High-pressure synthesis of a new silicon clathrate superconductor, Ba_8Si_{46}. Inorg. Chem. **39** (2000) 56–58.
[150] Fukuoka, H.; Kiyoto, J.; Yamanaka, S.: Superconductivity of metal deficient silicon clathrate compounds, $Ba_{8-x}Si_{46}$ ($0 < x \le 1.4$). Inorg. Chem. **42** (2003) 2933–2937.
[151] Demchyna, R.; et al.: Manuscript in preparation.
[152] Fukuoka, H.; Kiyoto, J.; Yamanaka, S.: Superconductivity and crystal structure of the solid solutions of $Ba_{8-\delta}Si_{46-x}Ge_x$ ($0 \le x \le 23$) with Type I clathrate structure. J. Solid State Chem. **175** (2003) 237–244.
[153] Demchyna, R.; Schnelle, W.; Burkhard, U.; Schwarz, U.; Grin, Yu.: High pressure and high temperature synthesis of quasibinary clathrate $Ba_6Ge_{25-x}Si_x$ ($0 < x < 25$). The 10th European Conference on Solid State Chemistry. August 29−September 1, Sheffield, United Kingdom (2005).
[154] Demchyna, R.; Köhler, U.; Prots, Yu.; Schnelle, W.; Baenitz, M.: Burkhardt, U.; Paschen, S.; Schwarz, U.: High-pressure synthesis and physical properties of the europium-substituted barium clathrate $Ba_{8x}Eu_xGe_{43}\square_3$ ($x \le 0.6$). Z. Anorg. Allg. Chem. **632** (2006) 73–78.
[155] Fukuoka, H.; Yamanaka, S.: Title: High-pressure synthesis and transport properties of a new binary germanide, $SrGe_{6-\delta}$ (δ congruent to 0.5), with a cagelike structure. Inorg. Chem. **44** (2005) 1460–1465.
[156] Fukuoka, H.; Yamanaka, S.: High-pressure synthesis and superconductivity of $LaGe_5$ containing a tunnel germanium network. Phys. Rev. B**67** (2003) 094501.
[157] Leger, J.-M.; Hall, H. T.: Pressure and temperature formation of A_3B compounds. I. Nb_3Si and V_3Al. J. Less Common Metals **32** (1973) 181–187.

[158] Popova, S. V.; Fomicheva, L. N.: Neorganicheskij Materialy **18** (1982) 251–255; New phases in Re–Ga and Os–Ga systems, obtained at a high-pressure. Inorg. Materials **18** (1982) 205–208.
[159] Killpatrick, D. H.: Pressure-temperature phase diagrams for Nb_3In and Nb_3Bi. J. Phys. Chem. Solids **25** (1964) 1213–1216.
[160] Fukuoka, H.; Yamanaka, S.: High-pressure synthesis and properties of a cerium germanide $CeGe_3$ with the cubic Cu_3Au type structure. Chem. Lett. **33** (2004) 1334–1335.
[161] Leger, J. M.; Hall, H. T.: Pressure and temperature formation of A_3B compounds Nab_3Ge, Nb_3Sn, Nb_3Pb, V–In and V–Pb. J. Less Common Metals **34** (1974) 17–24.
[162] Larchev, V. I.; Popopva, S. V.: New phases in the system Pt–Sn at high pressure. Inorg. Materials **20** (1984) 693–695.
[163] Miller, K.; Hall, H. T.: High-pressure synthesis of lutetium trilead. J. Less Common Metals **32** (1973) 275–278.
[164] Beister, H.-J.; Syassen, K.: Phase transition of Na_3As under pressure. Z. Naturforsch. **45b** (1990) 1388–1392.
[165] Yamaschita, T.; Takizawa, H.; Sasaki, T.; Uheda, K.; Endo, T.: Mn_3Sb: A new L1-type intermetallic compound synthesized under high-pressure. J. Alloys Comp. **348** (2003) 220–223.
[166] Tsvyashchenko, A. V.: High pressure synthesis of Yb_3T compounds (T = Co, Ni). J. Less Common Metals **118** (1988) 103–107.
[167] Range, K.-J.; Christl, E. G.: Hochdrucksynthese und Kristallstruktur von Pt_8Al_{21}, $Pd_8Al_{17}Si_4$ und Pt_8Al_{21}. J. Less Common Metals **136** (1988) 277–285.
[168] Popova, S. V.; Putro, V. G.: Neorganicheskij Materialy **15** (1979) 1210–1213; Crystal structure of alloys of the system Ta–Ga obtained at high pressure. Inorg. Materials **15** (1979) 947–949.
[169] Popova, S. V.; Fomichova, L. N.: High-pressure synthesis of molybdenum gallides. 3rd All-union conference on Crystal Chemistry of Intermetallic Compounds. Lvow, October 4–6, 1978.
[170] Popova, S. V.; Fomichova, L. N.: Crystallization of tungsten-gallium alloys at high pressure. J. Less Common Metals **77** (1981) 137–140.
[171] Larchev, V. I.; Popova, S. V.: The new chimney-ladder phases Co_2Si_3 and Re_4Ge_7 formed by treatment at high-temperatures and pressures. J. Less Common Metals **84** (1982) 87–91.
[172] Popova, S. V.; Fomicheva, L. N.: Synthesis of tungsten germanides at high-pressure. Inorg. Materials **14** (1978) 533–535.
[173] Takizawa, H.; Sato, T.; Endo, T.; Shimada, M.: High-pressure synthesis and electrical properties of Mn_3Ge_5 with $Mn_{11}Si_{19}$-type structure. J. Solid State Chem. **68** (1987) 234–238.
[174] Takizawa, H.; Sato, T.; Endo, T.; Shimada, M.: High pressure synthesis and electrical and magnetic properties of $MnGe_4$ and $CoGe_4$. J. Solid State Chem. **88** (1987) 384–390.
[175] Larchev, V. I.; Popova, S. V.: The new phases $IrSn_4$ and $RhGe_4$ formed by high-pressure treatment. J. Less Common Metals **98** (1984) L1–L3.
[176] Tsvyashchenko, A. V.: High pressure synthesis of RE_6Cu_{23} compounds (RE = Tb, Dy, Yb, Lu). J. Less Common Metals **99** (1984) L9–L11.
[177] Henry, P. F.; Weller, M. T.: Synthesis and crystal structure of Ca_3Au_4. J. Alloys Comp. **292** (1999) 152–155.